RESEARCH ARTICLE

Functional Ecology | BRITISH ECOLOGICAL SOCIETY

An aerodynamic perspective on hurricane-induced selection on *Anolis* lizards

Shamil F. Debaere[1] iD | Colin M. Donihue[2,3] iD | Anthony Herrel[1,4] iD |
Sam Van Wassenbergh[1] iD

[1]Department of Biology, University of Antwerp, Antwerp, Belgium

[2]Department of Biology, Washington University in St. Louis, St. Louis, MO, USA

[3]Institute at Brown for Environment and Society, Brown University, Providence, RI, USA

[4]Département Adaptations du Vivant, UMR 7179 C.N.R.S/M.N.H.N, Paris, France

Correspondence
Sam Van Wassenbergh
Email: sam.vanwassenbergh@uantwerpen.be

Abstract

1. Studies have demonstrated that hurricanes can drive selection in Neotropical anoles. In a recent study, it was shown that post-hurricane survivors showed longer toepad areas and, surprisingly, shorter femurs.

2. One potential explanation for the reduction in femur length is that increased drag on individuals with longer femurs causes them to be blown off their perch. Consequently, lizards with shorter femora might survive better in hurricanes.

3. To gain insight into the form–function relationships of drag reduction in perched lizards exposed to high-velocity winds, we quantified drag forces on *Anolis* lizard models in realistic grasping positions using computational fluid dynamics.

4. We showed that overall drag, as well as the relatively high drag at the hindlimbs strongly increase with the distance of the pelvic region from the perch. As optimal postures to resist sustained arboreal pulling involve extended limbs, longer hindlimbs increase the chance of having the limbs and pelvic region positioned outside the zone in which efficient shielding from the wind by the perch occurs.

5. Our study underlines the complexity of performance trade-offs on the evolution of limb morphology in arboreal lizards, and emphasizes the importance of generally ignored functions such as aerodynamic drag reduction in arboreal ecosystems.

KEYWORDS
biomechanics, clinging, drag force, fluid dynamics, lizards

1 | INTRODUCTION

Hurricanes can cause catastrophic damage and often have long-lasting effects on ecosystems (e.g. Spiller et al., 1998; Wiley & Wunderle, 1993). Two main factors influencing the impact and effects of hurricanes on terrestrial ecosystems are wind and rain. Intense rainfall may saturate the soil, causing flooding and erosion, while high-velocity winds may cause defoliation, breakage and the blowdown of trees in forest-dominated ecosystems (Tanner et al., 1991). The impact of hurricanes can be high among both plant and animal species, and may drastically alter species composition and the structure of ecosystems (e.g. Harcombe

et al., 2009; Pavelka et al., 2007; Wiley & Wunderle, 1993; Willig & Camilo, 1991). With the recent global temperature rise and increasing atmospheric CO_2 concentrations, future hurricane frequency, variability and intensity is expected to increase (Holland & Bruyère, 2013; Zhao et al., 2009).

Tree- and twig-dwelling *Anolis* lizards have recently become a model system to investigate natural selection caused by hurricanes (Donihue et al., 2018, 2020; Dufour et al., 2019; Rabe et al., 2020). Scansorial animals, particularly those inhabiting the tree canopy, are especially vulnerable to high-velocity hurricane winds. While survival of such an extreme weather event may be coincidental (i.e. random mortality), it was shown that directional phenotypic change

through natural selection occurs due to hurricanes in two populations of island lizards (Donihue et al., 2018).

However, elucidating functional interpretations of the observed phenotypic changes after a hurricane necessitates additional investigation. One trait, the mean relative toepad surface area of surviving anoles, was larger among the survivors than in the pre-hurricane population (Donihue et al., 2018). As a positive correlation between toepad size and clinging ability has previously been documented for *Anolis* (Dufour et al., 2019; Elstrott & Irschik, 2004), this mean toepad enlargement in a population struck by a hurricane was predicted a priori. On the other hand, unexpectedly, the relative hindlimb length of *Anolis* lizards decreased in the post-hurricane population compared to the pre-hurricane population (Donihue et al., 2018). In particular, relatively short femurs increased the chance of hurricane survival (Donihue et al., 2018). A study by Kolbe (2015) documented a positive effect of forelimb and hindlimb length on maximal clinging force on cylindrical perches, but could not exclude that this was due to the presumably larger toepads of individuals with longer legs rather than due to limb length per se. Consequently, how morphological factors other than toepad area influence clinging ability remain unclear, as does the reason for why shorter hind legs favour hurricane survival.

Alternatively, it has been hypothesized that aerodynamics may be responsible for hurricane-induced selection for shorter femora (Donihue et al., 2018). Longer hindlimbs may indeed induce increased drag on the lizard. When faced with simulated hurricane force winds in a field-experimental setting, anoles consistently position themselves vertically on the leeside of a perch, head up, forelimbs close to the body and hindlimbs extended or in a crouched position (Figure 1; Donihue et al., 2018). The larger exposed surface area of longer hindlimbs may make them more susceptible to catching wind, resulting in an increased likelihood that the lizard will be blown off its perch. In support of the assumption that the hindlimbs are the weakest link when faced with high-velocity winds while holding on to a perch, the hindlimbs were the first to lose contact with the perch in the majority of cases in an experimental setting using a high-power leaf blower as an artificial wind source (Donihue et al., 2018). In order to unravel the proximate causes of this unique example of morphological evolution by hurricane-induced selection in an arboreal ecosystem, we here test whether the femur is subjected to high drag forces in realistic gripping postures. Moreover, we evaluate in silico how femur elongation impacts the aerodynamic loading on the lizard.

2 | MATERIALS AND METHODS

2.1 | Perching posture modelling

In order to serve as input in the aerodynamic analysis described below, three-dimensional models were constructed using Geomagic
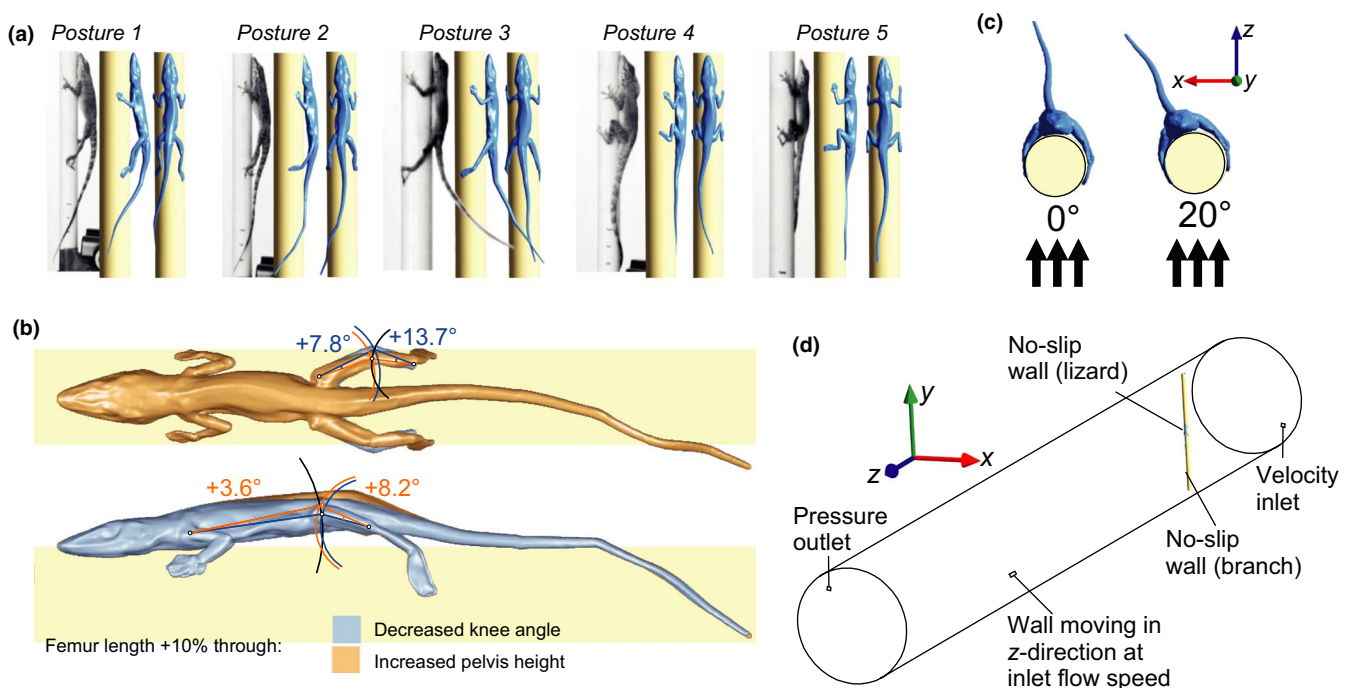
FIGURE 1 Model input for simulations of airflow over lizards that grip onto a vertical branch. In (a), three-dimensional surface reconstruction of *Anolis* in five realistic postures during exposure to strong wind coming from the left are illustrated. Image triplets show the master video image in lateral view (left), the laser scan-based 3D surface reconstruction in lateral view (middle) and in dorsal view (right). See Table 1 for a detailed description of the postures. In (b), the two scenarios (blue and orange colours) of morphological and postural change due to 10% femur length increase are shown in lateral view (bottom) and dorsal view (top). Changes in segment angles form the base model (posture 2 in Figure 1a) to the model with increased pelvis height (orange) and to the model with flexed knee angle (blue) are indicated in (b). In (c), the two simulated airflow directions are illustrated. In (d), the geometry of the flow domain for computational fluid dynamics is given, with indication of the boundary conditions

Wrap 2017 software (3D Systems Inc.) based on five video images of *Anolis scriptus* in a variety of postures while gripping onto a vertical pole of 20-mm diameter in an experimental simulation of hurricane-level winds (Donihue et al., 2018; Figure 1a). The choice of this perch diameter was based on the analysis from Donihue et al. (2018), who collected perch data in the field on the Turks and Caicos Islands. As a first step in the modelling process, a laser scan of a species with a similar morphology, *Anolis carolinensis* (snout–vent length = 58 mm), was made using a Faro Laser ScanArm V2 (Faro Technologies Inc.) mounted on a 1.8-m long, seven axis FaroArm Platinum arm. From the obtained triangulated surface mesh, the head, neck, trunk, tail and three segments per limb (e.g. for the hindlimb from proximal to distal: thigh, shank and foot) were carefully moved into a position that best matched the video images (Figure 1a). These operations involved cutting the original surface mesh, performing a series of rotations and translations and finally restitching the parts back into a continuous, watertight surface using Geomagic Wrap's curvature-based gap-bridging and hole-filling tools. The lizard's limb posture was assumed to be bilaterally symmetric, since only one side of the animal was visible from the lateral-view videos. Small details of the autopodia, namely digits and claws, were simplified. This seems justified as their overall contribution to aerodynamic loading will be small. Finally, all triangulated surface meshes of the lizards were converted into NURBS (non-uniform rational basis spline) surface patches using Geomagic Wrap. Doing so, patch edges were placed strategically to allow aerodynamic forces to be calculated on individual body parts (head, neck, trunk, tail and each limb's stylopodium, zeugopodium and autopodium).

The five modelled postures (postures 1 to 5) were ordered by decreasing distance of the pelvis from the perch. This separation between the pelvic girdle and the perch was quantified as the minimum distance between the perch surface and the ventrum at the level of the pelvic joint, and hereafter referred to as *pelvic distance*. All five postures were observed in performance trials and reflected the diversity of limb positions naturally assumed by the individuals in the study (Figure 1a). In these laboratory trials (Donihue et al., 2018), lizard generally started in a crouched position, while postures with more extended hindlimbs (i.e. larger pelvic distance) typically preceded the loss of hindlimb grip. A detailed description of the geometry of each posture is given in Table 1.

In order to evaluate the effect of a 10% increase in femur length on aerodynamic drag, the model of posture 2 was taken as a reference for two additional simulations in which the femurs were axially stretched by 10% (Figure 1b). Implementing this elongation will influence the position of the attached body parts—it will move the shank and feet laterally so that the feet will lose contact with the cylinder, and/or it will move the pelvic girdle more dorsally. Both situations are explored in the two additional models. Since the first option would give rise to aerodynamic artefacts due to the feet being strongly exposed to the wind, we kept the feet at the same positions and flexed the knees. For the second option, to avoid having to translate the entire trunk, forelimbs, neck and head in the dorsal direction, the angle of the trunk was adjusted and the knee

TABLE 1 Geometry of the five modelled grasping postures displayed in Figure 1a

Posture	Pelvic distance (mm)	Description
1	6	Strongly extended hindlimbs at a relatively large angle with the perch compared to the other postures. Head closely adhering to the perch. Wide grasp by the frontlimbs
2	2.8	Hindlimbs at a slightly sharper angle with the perch compared to posture 1. Closely adhering head, but in contrast to posture 1, the frontlimbs take a less wide grasp
3	0.6	Extended hindlimbs reach far around the perch
4	0.2	Hindlimbs remain close to the perch and are flexed
5	0.16	Flexed hindlimbs as in posture 4, but the frontlimbs are extended more anteriorly, and the head is slightly lifted

angle extended so that predominantly the pelvic region is translated dorsally. This results in two models with 10% elongated femurs, namely one with flexed knees and one with a dorsally shifted pelvic girdle (Figure 1b).

2.2 | Computational fluid dynamics

To evaluate the aerodynamic forces on the body and body parts in hurricane-like conditions, we applied the mathematical modelling technique of computational fluid dynamics (CFD). Similar to the experimental conditions of the work by Donihue et al. (2018), 30 m/s airflow was imposed over a vertical cylinder simulating a branch with the anole models placed on the leeside. Although in reality the wake would probably show time-varying patterns, time-independent (i.e. steady-state) Reynolds-averaged flow solutions were targeted, since gripping is predominantly an endurance task for which pinpointing the exact instantaneous force values is not critical, and time-averaged force magnitudes are assumed sufficient to evaluate the overall aerodynamic loading.

The surface models were imported in ANSYS 2019 R1 (ANSYS Inc.). A cylindrical outer boundary of 0.6 m in diameter and 5-m long was created to function as the virtual wind tunnel in which the lizard is placed more to the front to allow sufficient space for resolving the wake (Figure 1d). As boundary conditions, this part includes a 'velocity inlet' in the front (30 m/s inflow imposed) and a 'pressure outlet' in the back (zero pressure difference due to flow over the lizard and branch imposed). The cylindrical boundary sides are modelled as impermeable boundaries ('walls') that move along with the airflow. The lizard surface and the 20-mm diameter branch are modelled as smooth 'walls' for which the no-slip condition is enforced (Figure 1d).

The flow domain originally consisted of approximately 65 million tetrahedral mesh cells constructed in ANSYS Meshing. The minimum edge length of the mesh to apply to regions of the highest curvature on the lizard was set at 50 μm. Mesh element size was allowed to increase away from the lizard at a growth rate of 1.07 until reaching a maximum edge length of 25.6 mm. To improve mesh quality on sharp-angled surfaces, the tetrahedra were converted into polygon mesh cells in ANSYS Fluent. A mesh convergence test showed that, after substantial differences between coarser meshes, only a few percent of difference in drag force was calculated when refining the polygon face density on the lizard from 40 to 90 million/m^2. As the five different models (Figure 1a) had polygon densities between 47 and 78 million/m^2, we concluded that the meshes are adequate.

To account for the effects of turbulence associated with external flows at Reynolds numbers (Re) above 20,000 (here Re = 40,000 for a 20-mm branch thickness along the flow direction at 30 m/s air flow), the four-equation shear stress transport (SST) model was used in the CFD solver ANSYS Fluent. This model combines two commonly applied models (the k-ε model in the free stream and the k-ω model near the walls), and has shown to provide reliable results (e.g. for aerofoils at Re = 120,000; Aftab et al., 2016). As fluid, we used an air density of 1.225 kg/m^3 and viscosity of 1.7894 10^{-5} kg m^{-1} s^{-1}. The default solver settings of ANSYS Fluent 2019 R1 were used (SIMPLE scheme; least squares cell-based gradient treatment; second-order pressure discretization; second-order upwind for momentum; first-order upwind for turbulent kinetic energy, specific dissipation rate, intermittency and momentum thickness Re). Calculations were run for 2000 iterations on a computer with 36 processor cores. Iterative convergence was monitored for drag force on the lizard, together with the scaled residuals of the governing equations. The suitability of the settings was further verified by comparing the predicted drag coefficient (C_D; projected surface area as reference area) of a sphere in a CFD simulation (C_D = 0.405) with the results from wind and water tunnel experiments (C_D for subcritical Re between approximately 0.40 and 0.48; Hoerner, 1965). In order to account for minor variation in wind direction, simulations were solved for the lizard precisely at the leeside of the branch (0° simulations) and at a roll angle of 20° (Figure 1c). Since field measurement has shown that changes in wind angle over a short time (i.e. 1-min windows) typically do not exceed 20° for high-speed winds (Mahrt, 2011), the simulated range of 20° probably covers the natural variability in wind angles of attack on perched lizards during hurricanes. All reported results are from steady-flow models, which represent the mean aerodynamic load on the lizard. The validity of this approach was tested through an additional simulation of transient flow. This transient simulation showed that flow patterns in the relatively narrow and disorganized wake past the lizard are well-approximated by steady-flow models. Under time-dependent conditions, total drag force on the lizard, for example, showed fluctuations at about 50 Hz of ±5% around the reported mean of the steady-flow models (Figure S1). The reported drag forces include both pressure forces and viscous forces.

3 | RESULTS

When pooling data for all five postures and both wind angles (Figure 1), drag force was highest on the hindlimbs (34 mN), followed by the frontlimbs (19 mN), head (19 mN), trunk (18 mN), tail (17 mN) and neck (6 mN). The 20° wind angle simulations yielded 16% higher drag force on the entire body compared to the 0° simulations, and 10% higher for the pooled hindlimbs. Within the hindlimb, the drag force predominantly occurred at the thigh (97%), followed by the shank (14%). Net drag on the foot was, on average, absent (–11%; Figure 2).

Considerable variation occurred between the five postures (Figure 2). The two postures with the extended hindlimbs and a considerable gap between the pelvis and the perch, postures 1 and 2 (Figure 1a), experience the highest drag among the five postures (Figure 3). Postures 1 and 2 were the only of the five postures showing a notable positive (pushing) air pressure on the ventral side of the thighs in addition to the negative (sucking) pressure on their dorsal side (the latter was present in all simulations; Figure 2). The correlation between pelvic distance, defined as the minimal distance between the perch and the ventrum at the level of the pelvis, and drag force on the hindlimb (R^2 = 0.94; p = 0.006), as well as drag force on the pooled limbs and trunk (R^2 = 0.83; p = 0.031) was significant (Figure 3).

The models with 10% elongated femurs (Figure 1b) showed small overall differences in drag force with respect to the original model of position 2. The model with the 10% longer femurs and flexed knee angle had –1.6% overall drag force, +1% drag on the hindlimbs and +13% drag on the trunk. The model with the 10% longer femurs and higher pelvic distance had +1.5% overall drag, +13% drag on the hindlimbs and –23% drag on the trunk.

4 | DISCUSSION

Our analysis confirmed the importance of *Anolis* hindlimb morphology and posture from an aerodynamic perspective to withstand high wind forces while holding on to a perch, as was hypothesized previously (Donihue et al., 2018). Across the range of different postures that were analysed using CFD (Figure 1a), the hindlimbs came out as the body part experiencing the most drag force (Figure 2). Particularly, within the hindlimb, the thigh stood out as the primary wind-loaded segment. These results are in line with the observation that hurricanes induce a selection pressure towards shorter femurs.

However, a clear distinction appeared between crouched postures that keep the body close to the perch and postures with more extended hindlimbs in which the pelvic region is lifted off the perch. With overall lower drag, and virtually no drag force on the hindlimbs, crouched postures make efficient usage of the wind shielding by the perch (Figure 3). Maintaining this crouched, gripping posture under hurricane winds is optimal to reduce aerodynamic drag. Once the hindlimbs become more extended, strong aerodynamic forces will act on the pelvic region. Aerodynamic shielding by the perch
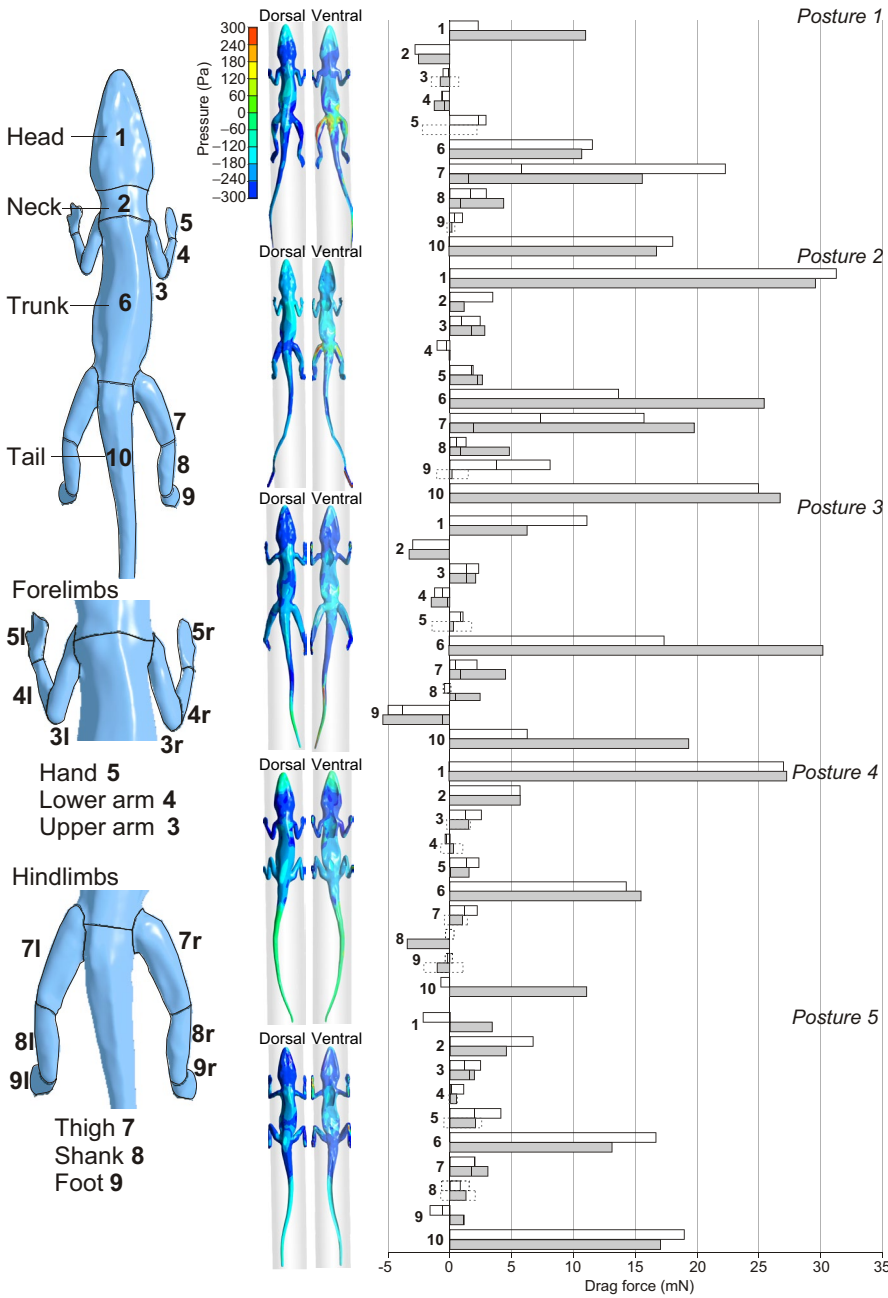
FIGURE 2 Computational fluid dynamics results of drag forces on different body parts. Body parts are numbered as indicated on the left. Wind speed is 30 m/s. The middle column shows aerodynamic pressure on the body in dorsal view (left) and ventral view (right) for the 0° wind angle simulations. Drag forces in the bar charts in the right column show drag forces per body segment for a 0° wind angle (white bars) and 20° wind angle (grey bars). Limb segment results are shown cumulative for left and right parts, with a dash inside the bars indicating the respective contributions of left and right. Dotted bars are shown in the case of drag forces with opposing signs on left and right limb segments. Postures 1 to 5 are illustrated in more detail in Figure 1a
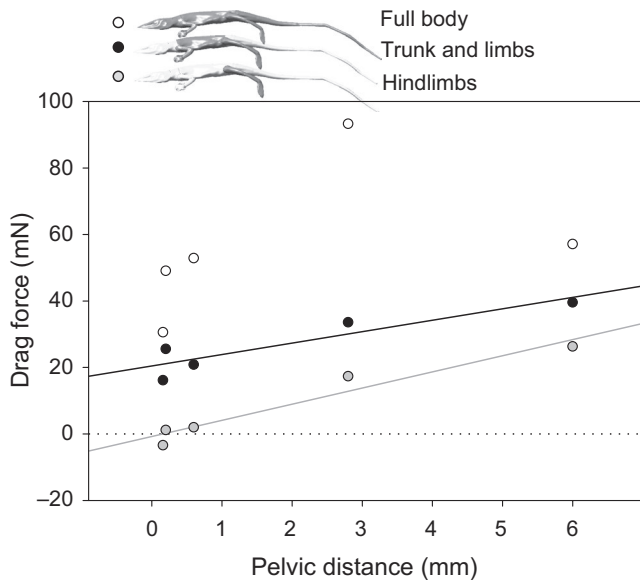
is clearly reduced when the vent is no longer adducted against the perch (Figures 2 and 3).

To explore this effect in more detail, we performed additional simulations with an elliptical cylinder as a simple model for the lizard's body, placed at a range of distances away from the perch (Figure 4). This analysis indicates that the 'no drag zone' extends to about one quarter of the diameter of the shielding perch. The crouched postures in our analysis (postures 2 to 5) are within this zone. Further separation from the perch causes drag force to rise steeply, and approximately linearly, and to reach about 30% of the unshielded drag force when separated by half a perch diameter (Figure 4).
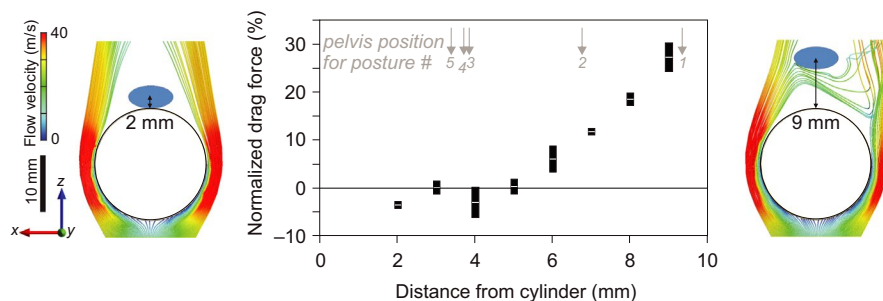
It can be expected that it will be more challenging for lizards with longer hindlimbs to keep a position in which the body is fully adducted against the perch. Maintaining a crouched posture requires active

muscle flexor activity to counter the drag force. Extended limb postures, on the other hand, can be maintained largely passively—once the gripping adhesion is established, the joints of the extended limb will passively transfer the aerodynamic forces to the gripping point to allow the lizard to remain immobile. This type of gripping with extended limbs typically results in maximal grasping force in arboreal vertebrates (Thomas et al., 2016). Based on the images of *Anolis scriptus* holding onto a vertical branch with an artificial wind source (Donihue et al., 2018), hands and feet are, on average, placed near the widest point on the branch (Figure 1a), presumably to exploit the strong adhesion of the toepad setae to resist forces parallel to the surface (Autumn et al., 2000; Stewart & Higham, 2014) as drag force will then pull the toepads parallel to the branch's surface. Once the legs become extended, either due to sustained drag forces or due

to a temporary high peak in drag force, the pelvic region will move further away from the branch compared to the pectoral region due to the longer hindlimbs relative to the forelimbs, thus exposing the pelvic region to higher drag forces. This may explain why the hindlimbs are generally the first to lose their grip (Donihue et al., 2018). Consequently, the longer the hindlimbs, the further the pelvic region will extend from the perch. In turn, this may subject lizards with longer hindlimbs to higher drag forces, and therefore may explain why shorter hindlimbs are advantageous in hurricane winds.

This intriguing interplay between adaptation for grasping and drag reduction under hurricane conditions remains open for further study. For example, how grasping endurance and posture is influenced by hindlimb anatomy, and how this is linked to hindlimb length remains an open question. *Anolis* species with longer hindlimbs have larger cross-sectional areas of their hindlimb muscles (Lowie et al., 2019), and may thus be capable of more forceful, active grasping in crouched positions, but the longer legged species may also have a larger overall body area exposed to the wind, which might cancel out this potential advantage. From an aerodynamic perspective, our CFD results for the models after elongation of the thigh by 10% (Figure 1b) did not completely confirm the insights from the comparison between postures (Figures 2 and 3), as the increase in drag force (+1.5%) was smaller than expected. Perhaps the current model simplifications may not have allowed us to recover such small-scale effects on aerodynamics. More accurate models of transient turbulent flows are probably needed to resolve this. Additionally, grasping conditions during hurricanes will vary from the standardized, smooth cylinder with flow perpendicular to its axis. Variation in, for example, angles of attack and perch diameter, as well as further insights into how perch diameter is related to grasping posture in lizards of different sizes could give a more complete view on aerodynamic conditions (Huey & Grant, 2020). However, despite these limitations, our analysis clearly points to a key role of drag reduction by exploiting aerodynamic shielding at the level of the hindlimbs.

FIGURE 3 Drag force as a function of distance of the pelvis from the branch. Results are shown for overall drag force (white circles), drag force on all limbs and the trunk (black circles) and drag force on the hindlimbs only (grey circles) at 30 m/s wind for the five postures shown in Figure 1a. Note especially that the drag on the hindlimbs strongly increases from near zero when the pelvic region is closely adducted against the perch (postures 5, 4 and 3; see Figure 1a) to a substantial proportion of the total drag in postures with the pelvis separated from the perch (postures 2 and 1; see Figure 1a)

AUTHORS' CONTRIBUTIONS

C.M.D., A.H. and S.V.W. conceived the study; S.F.D. and S.V.W. performed laser scanning, surface modelling, CFD simulations and drafted the manuscript; S.F.D. analysed the data. All the authors contributed to the editing of the final manuscript.

DATA AVAILABILITY STATEMENT

The CFD models and data supporting this article are available through the Dryad Digital Repository https://doi.org/10.5061/dryad.bk3j9kd9c (Debaere et al., 2021).

FIGURE 4 Computational fluid dynamics of 30 m/s air flow over an elliptical cylinder with lizard-body-like proportions at a range of different distances behind a cylindrical perch. The central graph shows drag forces, with boxes indicating drag fluctuation ranges in the final 10% of iterations. Corresponding pelvic distance from the five modelled postures (Figure 1a) is indicated by down arrows at the top of the graph. Note that below about one quarter of the shielding cylinder diameter, shielding from the airflow is complete. More distantly, drag force increases steeply in function of distance. Streamlines coloured by flow velocity are shown at the sides for the two extreme cases

ORCID

Shamil F. Debaere https://orcid.org/0000-0002-3951-3749
Colin M. Donihue https://orcid.org/0000-0003-1096-8536
Anthony Herrel https://orcid.org/0000-0003-0991-4434
Sam Van Wassenbergh https://orcid.org/0000-0001-5746-4621

REFERENCES

Aftab, S. M. A., Mohd Rafie, A. S., Razak, N. A., & Ahmad, K. A. (2016). Turbulence model selection for low Reynolds number flows. *PLoS ONE*, *11*, e0153755. https://doi.org/10.1371/journal.pone.0153755

Autumn, K., Liang, Y. A., Hsieh, S. T., Zesch, W., Chan, W. P., Kenny, T. W., Fearing, R., & Full, R. J. (2000). Adhesive force of a single gecko foot-hair. *Nature*, *405*, 681–685. https://doi.org/10.1038/35015073

Debaere, S., Donihue, C., Herrel, A., & Van Wassenbergh, S. (2021). Data from: An aerodynamic perspective on hurricane-induced selection on *Anolis* lizards. *Dryad Digital Repository*, https://doi.org/10.5061/dryad.bk3j9kd9c

Donihue, C. M., Herrel, A., Fabre, A.-C., Kamath, A., Geneva, A. J., Schoener, T. W., Kolbe, J. J., & Losos, J. B. (2018). Hurricane-induced selection on the morphology of an island lizard. *Nature*, *560*, 88–91. https://doi.org/10.1038/s41586-018-0352-3

Donihue, C. M., Kowaleski, A. M., Losos, J. B., Algar, A. C., Baeckens, S., Buchkowski, R. W., Fabre, A.-C., Frank, H. K., Geneva, A. J., Reynolds, R. G., Stroud, J. T., Velasco, J. A., Kolbe, J. J., Mahler, D. L., & Herrel, A. (2020). Hurricane effects on Neotropical lizards span geographic and phylogenetic scales. *Proceedings of the National Academy of Sciences of the United States of America*, *117*, 10429–10434. https://doi.org/10.1073/pnas.2000801117

Dufour, C. M., Donihue, C. M., Losos, J. B., & Herrel, A. (2019). Parallel increases in grip strength in two species of *Anolis* lizards after a major hurricane on Dominica. *Journal of Zoology*, *309*, 77–83. https://doi.org/10.1111/jzo.12685

Elstrott, J., & Irschick, D. J. (2004). Evolutionary correlations among morphology, habitat use and clinging performance in Caribbean Anolis lizards. *Biological Journal of the Linnean Society*, *83*(3), 389–398. https://doi.org/10.1111/j.1095-8312.2004.00402.x

Harcombe, P. A., Leipzig, L. E. M., & Elsik, I. S. (2009). Effects of hurricane Rita on three long-term forest study plots in east Texas, USA. *Wetlands*, *29*, 88–100. https://doi.org/10.1672/08-64.1

Hoerner, S. F. (1965). *Fluid-dynamic drag: Practical information on aerodynamic drag and hydrodynamic resistance*. Hoerner Fluid Dynamics.

Holland, G., & Bruyère, C. L. (2013). Recent intense hurricane response to global climate change. *Climate Dynamics*, *42*, 617–627. https://doi.org/10.1007/s00382-013-1713-0

Huey, R. B., & Grant, P. R. (2020). Lizards, toepads, and the ghost of hurricanes past. *Proceedings of the National Academy of Sciences of the United States of America*, *117*, 11194–11196. https://doi.org/10.1073/pnas.2006297117

Kolbe, J. J. (2015). Effects of hind-limb length and perch diameter on clinging performance in *Anolis* lizards from the British Virgin Islands. *Journal of Herpetology*, *49*, 284–290. https://doi.org/10.1670/13-104

Lowie, A., Gillet, E., Vanhooydonck, B., Irschick, D. J., Losos, J. B., & Herrel, A. (2019). Do the relationships between hindlimb anatomy and sprint speed variation differ between sexes in *Anolis* lizards? *Journal of Experimental Biology*, *222*, jeb188805. https://doi.org/10.1242/jeb.188805

Mahrt, L. (2011). Surface wind direction variability. *Journal of Applied Meteorology and Climatology*, *50*, 144–152. https://doi.org/10.1175/2010JAMC2560.1

Pavelka, M. S. M., Mcgoogan, K. C., & Steffens, T. S. (2007). Population size and characteristics of *Alouatta pigra* before and after a major hurricane. *International Journal of Primatology*, *28*, 919–929. https://doi.org/10.1007/s10764-007-9136-6

Rabe, M., Herrmann, N. C., Culbertson, K. A., Donihue, C. M., & Prado-Irwin, S. R. (2020). Post-hurricane shifts in the morphology of island lizards. *Biological Journal of the Linnean Society*, *130*, 156–165. https://doi.org/10.1093/biolinnean/blaa022

Spiller, D. A., Losos, J. B., & Schoener, T. W. (1998). Impact of a catastrophic hurricane on island populations. *Science*, *281*, 695–697. https://doi.org/10.1126/science.281.5377.695

Stewart, W. J., & Higham, T. E. (2014). Passively stuck: Death does not affect gecko adhesion strenght. *Biology Letters*, *10*, 20140701. https://doi.org/10.1098/rsbl.2014.0701

Tanner, E. V. J., Kapos, V., & Healey, J. R. (1991). Hurricane effects on forest ecosystems in the Caribbean. *Biotropica*, *23*, 513–521. https://doi.org/10.2307/2388274

Thomas, P., Pouydebat, E., Brazidec, M. L., Aujard, F., & Herrel, A. (2016). Determinants of pull strength in captive grey mouse lemurs. *Journal of Zoology*, *298*, 77–81. https://doi.org/10.1111/jzo.12292

Wiley, J. W., & Wunderle, J. M. (1993). The effects of hurricanes on birds, with special reference to Caribbean islands. *Bird Conservation International*, *3*, 319–349. https://doi.org/10.1017/S0959270900002598

Willig, M. R., & Camilo, G. R. (1991). The effect of Hurricane Hugo on six invertebrate species in the Luquillo Experimental Forest of Puerto Rico. *Biotropica*, *23*, 455–461. https://doi.org/10.2307/2388266

Zhao, M., Held, I. M., Lin, S.-J., & Vecchi, G. A. (2009). Simulations of global hurricane climatology, interannual variability, and response to global warming using a 50-km resolution GCM. *Journal of Climate*, *22*, 6653–6678. https://doi.org/10.1175/2009JCLI3049.1

SUPPORTING INFORMATION

Additional supporting information may be found online in the Supporting Information section.